How to cite: *Angew. Chem. Int. Ed.* **2023**, *62*, e202304088
doi.org/10.1002/anie.202304088

Cluster Compounds

Probing Charge-Transfer Processes in a Covalently Linked [Ge_9]-Cluster Imine Dyad

*Christoph Wallach, Yasmin Selic, Felix S. Geitner, Ajeet Kumar, Erling Thyrhaug, Jürgen Hauer, Antti J. Karttunen, and Thomas F. Fässler**

Abstract: C_{60} donor dyads in which the carbon cage is covalently linked to an electron-donating unit have been discussed as one possibility for an electron-transfer system, and it has been shown that spherical [Ge_9] cluster anions show a close relation to fullerenes with respect to their electronic structure. However, the optical properties of these clusters and of functionalized cluster derivatives are almost unknown. We now report on the synthesis of the intensely red [Ge_9] cluster linked to an extended π-electron system. $[Ge_9\{Si(TMS)_3\}_2\{CH_3C{=}N\}\text{-}DAB(II)^{Dipp}]^-$ (**1**$^-$) is formed upon the reaction of $[Ge_9\{Si(TMS)_3\}_2]^{2-}$ with bromo-diazaborole $DAB(II)^{Dipp}$-Br in CH_3CN (TMS = trimethylsilyl; DAB(II) = 1,3,2-diazaborole with an unsaturated backbone; Dipp = 2,6-di-*iso*-propylphenyl). Reversible protonation of the imine entity in **1**$^-$ yields the deep green, zwitterionic cluster $[Ge_9\{Si(TMS)_3\}_2\{CH_3C{=}N(H)\}\text{-}DAB(II)^{Dipp}]$ (**1-H**) and vice versa. Optical spectroscopy combined with time-dependent density functional theory suggests a charge-transfer excitation between the cluster and the antibonding π* orbital of the imine moiety as the cause of the intense coloration. An absorption maximum of **1-H** in the red region of the electromagnetic spectrum and the corresponding lowest-energy excited state at $\lambda = 669$ nm make the compound an interesting starting point for further investigations targeting the design of photo-active cluster compounds.

Introduction

Solar energy conversion is becoming increasingly important and points for the necessity to investigate photo-induced electron transfer in donor-acceptor systems and the construction of molecular electronic and optoelectronic devices.[1] Fullerenes are widely discussed as photo-sensitizing electron acceptors with respect to a wide variety of electron donors. C_{60} donor dyads, in which the carbon cage is covalently linked to an electron-donating unit have been discussed as one possibility for an electron-transfer system.[1,2] Since C_{60} molecules show structural and electronical similarities with homoatomic deltahedral *Zintl* ions of Group 14 elements,[3–7] we investigate the synthesis and optical properties of the corresponding functionalized [Ge_9] clusters. Solutions of $[Ge_9]^{4-}$ clusters are readily accessible by extraction of solid K_4Ge_9 and serve as precursors for the attachment of organic ligands with specific functions to the [Ge_9] cluster core. The straightforward production of the twofold silylated [Ge_9] cluster, its moderate steric shielding and the remaining negative charge of −2 allow for a follow-up chemistry of the dianion $[Ge_9\{Si(TMS)_3\}_2]^{2-}$ as a precursor. Consequently mixed-functionalized clusters bearing covalently bound group 13,[8] 14,[9–11] or 15[12–14] element-based fragments have become accessible, leading for example to a coupling of two cluster entities via a rigid silane.[15] The decoration of the twofold silylated cluster with phosphanyl fragments accounts for the introduction of Lewis basic functional groups to the cluster,[12–14] and also the threefold phosphanylated species $[Ge_9\{P(N^iPr_2)\}_3]^-$ has been reported.[16] Furthermore, the bare [Ge_9] cages can be functionalized with organic ligands, leading to the formation extend systems such as the dimeric vinylated cluster $[(CH{=}CH_2)\text{-}Ge_9\text{–}Ge_9(CH{=}CH_2)]^{4-}$.[17]

A few previous investigations indicated some interesting optoelectronic properties of [Ge_9] clusters. The formation of green tetramers $[Ge_9{=}Ge_9{=}Ge_9{=}Ge_9]^{8-}$ [18–20] and polymers $^1{}_\infty\{[Ge_9]^{2-}\}$[21,22] from red to brown $[Ge_9]^{4-}$ solutions have been reported, and UV/Vis spectroscopic investigations showed the relationship between the optical properties of bare deltahedral germanide clusters and fullerenes.[23] However, a targeted synthesis of oxidized [Ge_9] species is hampered by the formation of by-products and low yields. An investigation of the optical properties of silylated clusters $[Ge_9\{Si(TMS)_3\}_3]^-$ by means of ultrafast transient absorption spectroscopy (TA) revealed a photo-excitation-induced transfer of cluster electrons to the

[*] Dr. C. Wallach, M. Sc. Y. Selic, Dr. F. S. Geitner, A. Kumar, Dr. E. Thyrhaug, Prof. Dr. J. Hauer, Prof. Dr. T. F. Fässler
TUM School of Natural Sciences, Department Chemie, Technische Universität München
Lichtenbergstraße 4, 85747 Garching (Germany)
E-mail: thomas.faessler@lrz.tum.de
Prof. Dr. A. J. Karttunen
Department of Chemistry and Materials Science, Aalto University
00076 Aalto (Finland)

solvent or ligand environment, and, as a result, the generation of a transient $[Ge_9]^0$ species.[24,25] Similar interesting findings were reported for the transition metal-decorated species $[Ge_9\{Si(TMS)_3\}_3FeCp(CO)_2]$.[26]

An extension of the electronic system has been realized in so called *Zintl* triads,[5–7] in which two $[Ge_9]$ clusters are interconnected by a conjugated hydrocarbon chain, such as reported for $[R\text{-}Ge_9\text{–}(CH{=}CH\text{–}CH{=}CH)\text{–}Ge_9\text{-}R]^{4-}$ (R = $CH{=}CH_2$);[7] however, no optical properties have been reported. Due to the beneficial properties of silylated $[Ge_9]$ clusters we aimed for the introduction of a ligand with an electronic π-system near the cluster core, thereby possibly allowing charge transfer processes between the negatively charged cluster and the ligand sphere. We took advantage on the recently reported attachment of imines to the twofold silylated cluster, whereby unsaturated organic moieties could be introduced,[27] and report here on the anion $[Ge_9\{Si(TMS)_3\}_2\{CH_3C{=}N\}\text{-}DAB(II)^{Dipp}]^-$ (**1**$^-$) with an imine ligand inserted between the cluster and a diazaborole group. Protonation of the imine group of the intensely red cluster led to the generation of a zwitterionic cluster $[Ge_9\{Si(TMS)_3\}_2\{CH_3C{=}N(H)\}\text{-}DAB(II)^{Dipp}]$ (**1-H**) showing a bathochromic shift of the reaction mixture from deep red to green. We further performed a combined steady-state and transient optical spectroscopy/quantum chemistry study of **1-H**, where we account for its electronic structure and identify a charge-transfer excitation between the $[Ge_9]$ cluster and the iminium entity.

Results and Discussion

Synthesis of 1$^-$ and 1-H

The reaction of the twofold silylated cluster $[Ge_9\{Si(TMS)_3\}_2]^{2-}$ with equimolar amounts of the sterically hindered bromo-1,3,2-diazaborole DAB(II)^{Dipp}-Br [(II)= unsaturated backbone] in CH_3CN as a solvent yielded the anion $[Ge_9\{Si(TMS)_3\}_2\{CH_3C{=}N\}\text{-}DAB(II)^{Dipp}]^-$ (**1**$^-$) with an imine fragment located between the cluster and the boranyl moiety.[27] The N atom of the nitrile binds to the B atom of the diazaborole moity, whereas one cluster vertex Ge atom is connected to the electrophilic C atom adjacent to the N atom, causing the formation of an N–B (under cleavage of a B–Br bond) and a Ge–C bond, respectively (Scheme 1).[27] Experimental details are given in the Supporting Information. ESI mass spectroscopy reveals a mass peak of **1**$^-$ at m/z 1577.9 (Supporting Information, Figure S11 and S12). In the ^{1}H NMR spectrum the singlet of the hypersilyl protons are shifted from $\delta = 0.16$ ppm ($[Ge_9\{Si(TMS)_3\}_2]^{2-}$) to 0.22 ppm (thf-$d_8$), with the cluster protons, the protons of the boranyl entity, and that of the incorporated imine fragment in a ratio of 1:1:1.

Solutions containing the anion **1**$^-$ instantly turn green, when exposed to moisture. Addition of equimolar amounts of the soft acid NEt_3·HCl to a toluene solution of **1**$^-$ yields after eight hours a green reaction solution (Scheme 1). The mass peak of the charge-neutral compound **1-H** was detected in LIFDI-MS measurements at m/z 1578.9 (Figure S13), revealing a mass difference of exactly one hydrogen atom in comparison to ESI-MS measurements of the anion **1**$^-$.[28] The ^{1}H NMR spectrum shows a shift of the signal at $\delta = 0.22$ ppm in **1**$^-$ to 0.28 ppm, and the ^{11}B NMR signal is shifted from $\delta = 22.3$ ppm (**1**$^-$) to 18.6 ppm. The ^{1}H NMR signal observed at $\delta = 9.82$ ppm indicated the protonation of the anion and the formation of $[Ge_9\{Si(TMS)_3\}_2\text{-}\{CH_3C{=}N(H)\}\text{-}DAB(II)^{Dipp}]$, **1-H**. NMR spectra are given in Supporting Information in Figures S3 to S10.

Red and green crystals of the potassium salt of **1**$^-$ (**1-K**) and compound **1-H**, respectively, were obtained from diethyl ether and hexane solutions, with the unit formula comprising two diethyl ether molecules and one hexane molecule, respectively. Both compounds crystallize in the monoclinic space group $P\bar{1}$ with two formula units per unit cell, and the single crystal structure determination confirmed the molecular formula of **1**$^-$ and **1-H** (Figure 1). Crystallographic details are given in the Supporting Information (Table S1).[29] The iminium hydrogen atom of compound **1-H** was derived from the difference Fourier electron density map and was refined without constraints. The shape of the $[Ge_9]$ cluster cores in **1-K** and **1-H** are both best described as distorted tricapped trigonal prisms,

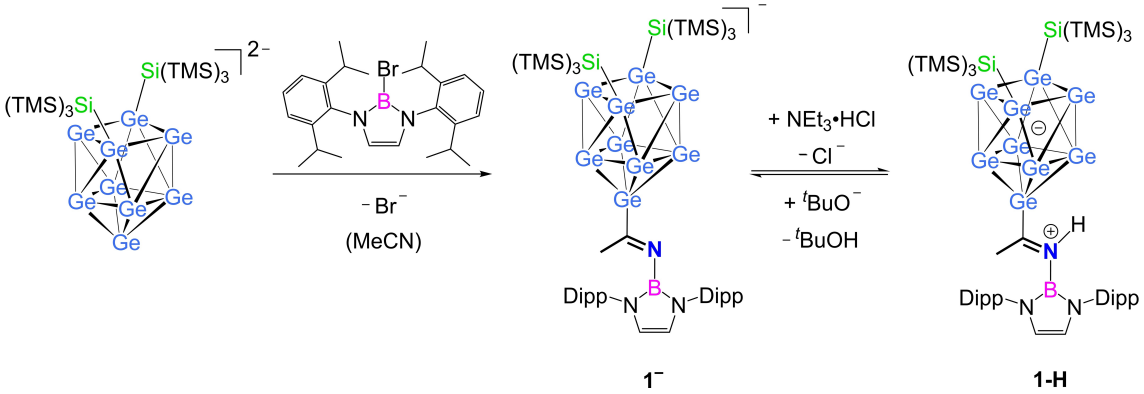

Scheme 1. Schematic presentation of the synthesis of **1**$^-$ starting from $[Ge_9\{Si(TMS)_3\}_2]^{2-}$ and the bromo-diazaborole DAB(II)^{Dipp}-Br, and the subsequent reversible protonation of **1**$^-$ by NEt_3·HCl, yielding **1-H**.

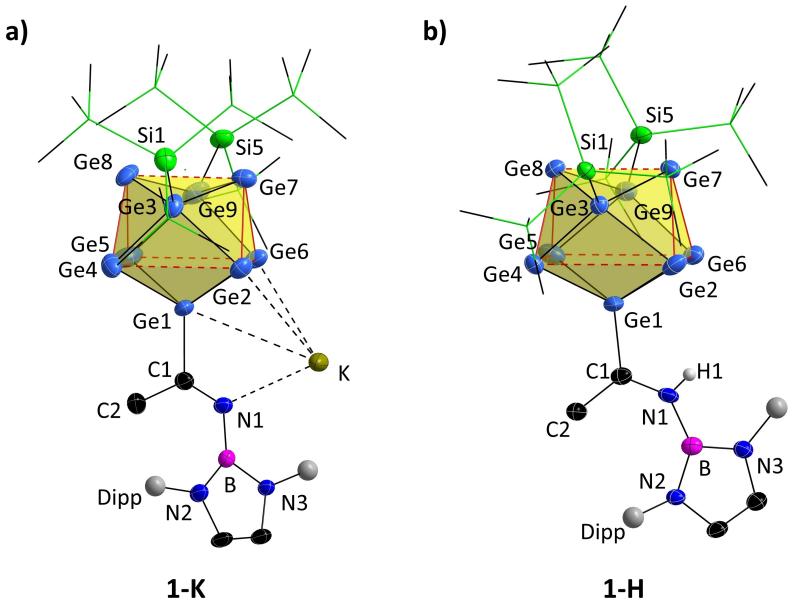

Figure 1. Molecular structures of a) **1-K** and b) **1-H**. All ellipsoids are shown at a 50% probability level. For clarity, hydrogen atoms (except H1), and co-crystallizing solvent molecules are omitted. The Dipp wingtips are illustrated as grey spheres. In (a) and (b) only the major occupied part of the disordered hypersilyl group Si5 is presented, TMS groups are presented as wire-sticks. Trigonal prismatic bases are indicated by red lines. Full ellipsoid plots of the structures are provided in the Supporting Information (Figures S1 and S2).

with the two prism heights Ge2–Ge4 and Ge5–Ge6 being elongated if compared to Ge7–Ge8, resulting in slightly distorted C_{2v}-symmetric clusters (Tables 1 and S2). The trigonal prisms and the prism heights are indicated by solid and dashed red lines in Figure 1, respectively. The two hypersilyl groups and the imine fragment bind to three Ge atoms that cap the rectangular faces of the trigonal prism. In each compound one of the hypersilyl groups is disordered, which is illustrated in detail in the Supporting Information, together with full ellipsoid plots of the molecules (Figures S1 and S2). All Ge–Ge and Ge–Si bond lengths are in accordance with previously reported data.[27,30,31]

1-K contains a polyhedral cluster anion that coordinates with a triangular face and the N atom of the ligand to a potassium cation, whereas charge neutral **1-H** is best described as a zwitterion with a negative charge on the three-fold substituted [Ge_9] cluster and a positive charge at the four-bonded nitrogen atom of the iminium moiety. Both compounds comprise a C=N double bond with a C–N distance of 1.280 and 1.325 Å, respectively. The C–N1 distance in **1-H** is elongated if compared to that in **1-K**, but it is still in the range of a formal C=N double bond.[32] This bond elongation correlates with a shorter Ge1–C1 distance in **1-H** (Table 1), which, however, is in range of various reported Ge–C single bonds.[33–36] Slightly elongated C=N bonds have previously been reported for molecules comprising cationic iminium moieties.[37] The C=N double bond character in **1-K** and **1-H** is confirmed by the planar coordination of C1 by Ge1, N1 and C2, showing for both compounds the sum of bond angles around C1 of perfect 360.0° and featuring also dihedral angles $\omega_{C2-C1-Ge1-N1}$ of approximately 180° (Table 1). **1-H** is also the first transition metal-free, charge neutral [Ge_9] cluster bearing only three substituents.

Table 1: Selected distances and angles in compounds **1-K** and **1-H**.

distance [Å]	1-K	1-H
Ge1–C1	1.985(5)	1.912(3)
C1–N1	1.280(6)	1.325(4)
C1–C2	1.501(7)	1.487(4)
B1–N1	1.448(6)	1.464(4)
angle [deg]		
N1–C1–Ge1	120.3(3)	118.6(2)
C2–C1–Ge1	115.1(3)	122.3(2)
C2–C1–N1	124.6(4)	119.1(3)
C1–N1–B1	126.0(4)	137.2(3)
C1–C2–*R*	109.5(4)	109.5(3)
$\omega_{C2-C1-Ge1-N1}$	180.0	179.8

Reversibility of the zwitterion formation

The reaction of a green toluene solution of **1-H** with equimolar amounts of the base KO^{t}Bu led to a color change from green to red within a few minutes (Figure S28). ^{1}H NMR spectroscopic investigations in C_6D_6 corroborated the formation of the monoanionic cluster $\mathbf{1}^-$ upon adding a thf-d_8 solution of the base to the green complex in a NMR tube. The reversible process is depicted in Scheme 1. Indicative of the reversibility of the protonation are the decay of the NH signal intensity at $\delta =$ 9.95 ppm and the shift of the hypersilyl protons from $\delta =$ 0.47 ppm (**1-H**) to 0.51 ppm ($\mathbf{1}^-$) (Figure S27). Further-

more, the process was studied by time-resolved UV/Vis absorption experiments. The decay of the absorption at 671 nm was monitored upon the injection of a KO^{t}Bu solution to a stirred toluene solution of **1-H** (Figure 2a).

The initial absorption was measured for approximately half a minute to exclude self-degradation, prior the addition of the base, which then leads almost instantaneously to a drop in the absorption intensity. The addition of 5 and 10 equivalents of KO^{t}Bu yielded almost identical time-dependent degradation curves (Supporting Information Figure S29) anticipating a pseudo-first order kinetic. Rate constants k were derived through a linear regression from $A = A_0 e^{-kt}$ by plotting $\ln(A/A_0)$ over t (A = absorption, k = rate constant, t = time; Figures 2b and Supporting Information Figure S30).[38] The rate constant adopts values of 26.5 min^{-1} (mean value of three measurements) and 30.6 min^{-1} (single measurement), for the application of 5 and 10 equivalents of KO^{t}Bu, respectively. The respective approximate half-lifes are $\ln(2)/k = 1.6$ and 1.3 s, respectively. Upon mixing [2.2.2]cryptand to the KO^{t}Bu solution before addition to the cluster, the consecutive deprotonation proceeds significantly faster (Supporting Information Figure S31). In conclusion, the basicity of the O^{t}Bu$^-$ anion is larger than that of the imine moiety in **1-H**. For comparison, bare $[Sn_9]^{4-}$ clusters show a larger basicity than O^{t}Bu$^-$, since the species $[Sn_9\text{–}H]^{3-}$ is not deprotonated by the same base.[39]

Optical spectroscopy

To further investigate the color change induced by the protonation of the imine group, we measured the optical spectra of **1**$^-$ and **1-H** in solutions of different polarity. As seen in Figure 3a, the anion **1**$^-$ features a broad absorption band at approximately 248 nm (5.0 eV, ε = 40286.2 M^{-1}cm^{-1}) in thf solution. Note that even rather small organic molecules are absorbing in this spectral range, and as a result it is often difficult to conclusively assign the spectra to specific species. Here, in particular, we observe that the spectrum of **1**$^-$ does not differ dramatically from those of the precursor ligand DAB-(II)^{Dipp}-Br, the reactant $[Ge_9\{Si(TMS)_3\}_2]^{2-}$, or species with other aromatic or heterocyclic ligands (Supporting Information Figures S18–S23).[24,25] Thus, while the observed spectrum would involve both cluster-centred and DAB(II) centred transitions, the spectral congestion means that no deconvolution into transitions to distinct excited states is possible.

The optical properties of **1-H** differ strongly from this picture, as can be seen from the spectra in Figure 3b. As suggested by its green color, the main absorption of **1-H** in toluene solution appears as a broad band at 671 nm (1.85 eV) with moderate oscillator strength (ε = 14237.0 M^{-1}cm^{-1}), followed by weaker transitions in the blue-to-near UV region at 387 and 437 nm (3.2 eV and 2.8 eV). Interestingly, changing the solvent from toluene to the more polar thf results in a blue-shift of the lowest-energy absorption band maximum of approximately 20 nm —reaching a center wavelength of 657 nm. Such a solvatochromic shift upon the change of the dielectric environment is generally indicative of optical transitions with charge-transfer character. In the present case, a shift to higher energy at increasing polarity suggests that the ground state of the **1-H** cluster carries a larger dipole moment than its excited-state. This is consistent with a molecular picture where photoexcitation of **1-H** involves the movement of the charge from a negatively charged Ge cluster moiety towards a positively charged N1 nitrogen of the DAB(II) ligand (Figure 1). In agreement with this, in hexane the absorption maximum shift further to the red, reaching 678 nm (1.83 eV, Figure 3b).

In order to further investigate the dynamics of **1-H** upon excitation, techniques with sufficient temporal resolution for the observation of the typically very rapid excited state relaxation processes are necessary. **1-H** is non-luminescent, ruling out techniques such as time-correlated single photon counting to investigate these processes. Instead, we rely on ultrafast transient absorption spectroscopy (TA) to follow the excited-state dynamics by

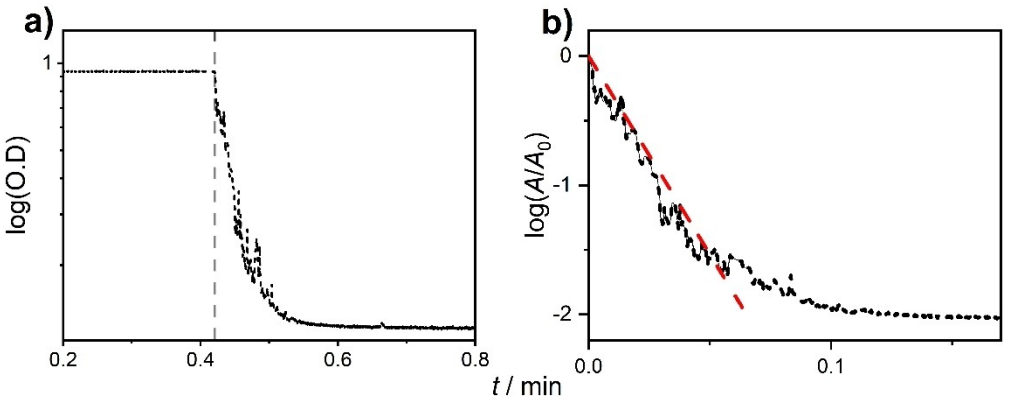

Figure 2. a) Time-dependent absorption of **1-H** monitored at 671 nm. At t = 0.4 min (dashed vertical line) 5 equivalents KO^{t}Bu are added to the stirred solution. b) Plot for the determination of the rate constant k (30.7 min^{-1}). Recorded data is presented in black, the linear regression is indicated by a red line. Spikes in the data are caused by the stirring bar.

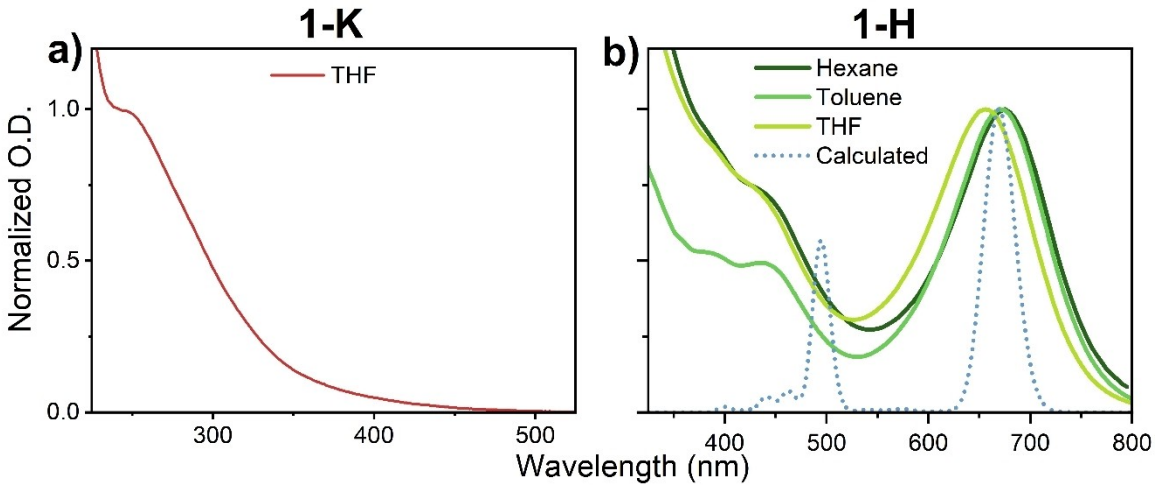

Figure 3. a) UV/Vis absorption spectrum of $\mathbf{1}^-$ in thf solution, showing a shoulder at $\lambda = 248$ nm (5.0 eV). b) UV/Vis absorption spectra of **1-H** in thf (657 nm), toluene (671 nm) and hexane (678 nm), showing solvent polarity dependent absorption maxima in the range of 1.89 eV to 1.83 eV. The calculated absorption spectrum of **1-H**, obtained at the DFT-BP86/TZVP level of theory,[40–44] is shown as dotted line and shows maxima at $\lambda = 495$ nm (2.14 eV, transition $S_0 \rightarrow S_8$) and $\lambda = 669$ nm (1.85 eV, transition $S_0 \rightarrow S_2$). The calculated spectrum is based on the vertical excitation energies of the 30 lowest-energy singlet excited states (the shortest calculated wavelength was 396 nm).

monitoring the excitation-induced changes in the optical absorption spectrum. Briefly, our TA instrument is based on the supercontinuum output of an argon-filled hollow-core fiber (HCF, Ultrafast Innovations) driven by an amplified Ti:Sapph laser (Coherent Legend). After splitting of the broadband HCF output into pump- and probe-pulses followed by filtering and compression, the system yields approximately 20 fs excitation pulses centered at 650 nm and white light probe pulses covering approximately the range of 350–850 nm (see Supporting Information Figures S24–S26 for details).

The detection wavelength versus time delay transient data obtained from a **1-H** solution in THF are shown in Figure 4a, from which conventional transient spectra at selected time delays are extracted and shown in Figure 4b. Immediately on excitation, the expected ground state bleach (GSB) and stimulated emission features (SE) around the absorption maximum at 657 nm are observed. These signals are accompanied by a broad excited state absorption (ESA) band in the green/blue spectral region around 500 nm. Within a few hundred femtoseconds, the signal decays at the red edge of the SE/GSB features, and a red/NIR ESA feature appears. These spectral changes can

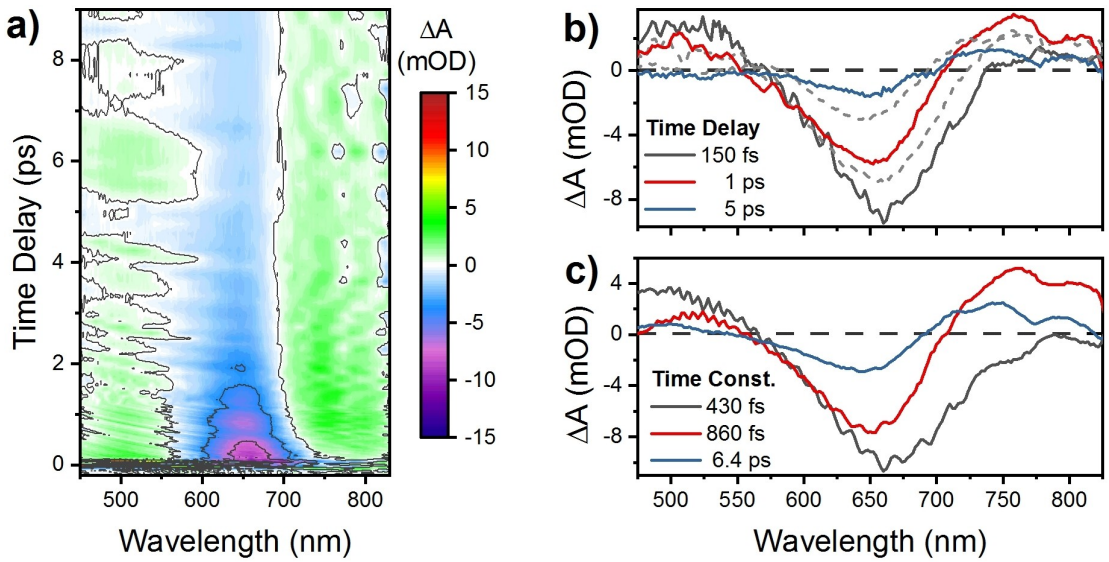

Figure 4. Transient absorption data of the cluster **1-H** in THF solution. a) Raw data over the first 9 ps after excitation at 650 nm plotted on probe-delay vs detection wavelength scale, b) transient absorption spectra extracted at selected time delays, c) evolutionary-associated decay spectra (EADS) and related time constants extracted by a global kinetic fit to the data.

be assigned to rapid thermalization within the manifold of (electronic and vibrational) states populated by the broadband excitation pulse as well as inertial solvation dynamics. The "quasi-relaxed" spectrum after these initial relaxation processes can subsequently be observed to decay on a low picosecond timescale, resulting in a full recovery of the ground state within approximately 10 ps. Although short-lived, the observed excited state lifetimes are comparable to other Ge clusters.[24] At the same time, lifetimes in the tens of ps are not unusual for systems involving substantial charge-transfer processes.

In order to gain quantitative insight into these processes, we further analyzed the transient dynamics using a global kinetic analysis approach. Here, we rely on singular-value decomposition of the data to identify the necessary number of unique fit components, followed by a fit of the data at each detection wavelength to a simple sum-of-exponential-decays model with a global constraint on the component lifetimes.[45] The results of this fitting procedure are shown in Figure 4c, revealing the characteristic lifetimes and the so-called evolutionary-associated decay-spectra (EADS) of the three unique components suggested by the singular value decomposition (SVD) analysis. Here, the kinetic model describes strictly unidirectional transfer through a sequence of N "compartments"—where N (in our case 3) is the number of unique components in the fit.

While clearly a simplified model, the EADS provides useful quantitative information on the spectral dynamics. Here, the early time relaxation involving a narrowing of the GSB/SE can be seen, as well as a loss of overall signal strength within 430 fs. This is followed by a bi-modal decay of the overall signal in parallel with more subtle changes in the ESA spectral shapes. Finally, the remaining relatively small fraction of the initially excited clusters decays back to the ground-state with a time-constant of 6.4 ps. While further studies are necessary to extract a detailed physical picture of the excited state behavior of **1-H**, the complicated behavior of the data suggests that there exist at least two distinct relaxation pathways from the excited state back to the ground state, and we further speculate that losses of SE and ESA may in part be due to population transfer into optically dark states.

Quantum chemical investigations

For a deeper understanding of the electronic properties of **1-H**, we applied density functional theory (DFT-BP86/TZVP level of theory and time-dependent DFT, TD-DFT)[40–44] and optimized the geometry of the compound starting from the single crystal structure data and calculated the 30 lowest energy vertical excitations. As seen in Figure 3b, the most intense signals in the calculated absorption spectrum are the $S_0 \rightarrow S_2$ transition observed at 669.0 nm (1.85 eV), followed by the $S_0 \rightarrow S_8$ transition at 495 nm (2.14 eV). The longer-wavelength absorption band matches well with the experimentally observed maximum at 671 nm. The shorter-wavelength absorption at 495 nm is red-shifted by approximately 0.3 eV in comparison to the experimentally observed shoulder at 437 nm. The $S_0 \rightarrow S_8$ excitation is more delocalized compared to the $S_0 \rightarrow S_2$ excitation (Supporting Information Figures S32 and S33), and TD-DFT calculations typically show larger errors when the extent of charge transfer increases.[46] The red species $\mathbf{1}^-$ absorbs light of wavelengths below 350 nm, and a detailed TD-DFT investigation of the high-energy excited states was not carried out.

The molecular orbital analysis revealed that the HOMO of compound **1-H** is based at the [Ge_9] core and extends to the atom C1, which is covalently bound to the cluster (Figure 5a). The LUMO is mostly located at the atoms C1 and N1, thus forming the anti-bonding π* orbital of the C=N double bond (Figure 5b). The HOMO–LUMO gap was calculated to 1.40 eV (886 nm).

According to the molecular orbital analysis a charge transfer from the formally negatively charged cluster into the antibonding π* orbital of the imine moiety is theoretically feasible. Indeed, TD-DFT calculations reveal that the electron density at the [Ge_9] moiety is reduced during the $S_0 \rightarrow S_2$ excitation at 669 nm, while the electron density at the C1 atom increases. This is in good qualitative agreement with our observations from the optical experiments revealing solvatochromism. The electron density change during the excitation is presented in Figure 5c, in which yellow and red color indicate decreasing and increasing electron density, respectively. Figure 5d schematically shows the charge transfer during the $S_0 \rightarrow S_2$ excitation of the zwitter ion **1-H**. Electron density is mainly transferred from the cluster to the electrophilic C1 atom of the imine ligand. For the calculated $S_0 \rightarrow S_8$ transition at 495 nm a similar change in the electron density at the atom C1 is observed, however, here also the boranyl ligand, which is a spectator ligand in the $S_0 \rightarrow S_2$ excitation, is participating by donating electron density into the system. Further graphical illustrations of the excitations can be found in the Supporting Information (Figure S32 and S33). In conclusion, the absorption maximum of **1-H** in the red region of the electromagnetic spectrum and the corresponding lowest-energy optically bright excited state at $\lambda = 669$ nm make the compound an interesting starting point for further investigations targeting the design of light-harvesting cluster compounds.

Conclusion

Herein we describe the reversible formation of the metal-free *Zintl* cluster zwitterion **1-H** by protonation of the imine functionality in anion $\mathbf{1}^-$. The intense green color of **1-H** is caused by charge transfer processes between the cluster and the antibonding π* orbital of the imine moiety as corroborated by quantum chemical calculations. Tailoring the electronic situation at the imine fragment is subject of forthcoming studies, aiming for a targeted control of the light-absorbing properties of the cluster compound, which can be seen as a first step on the way to the design of cluster-based light harvesting molecules.

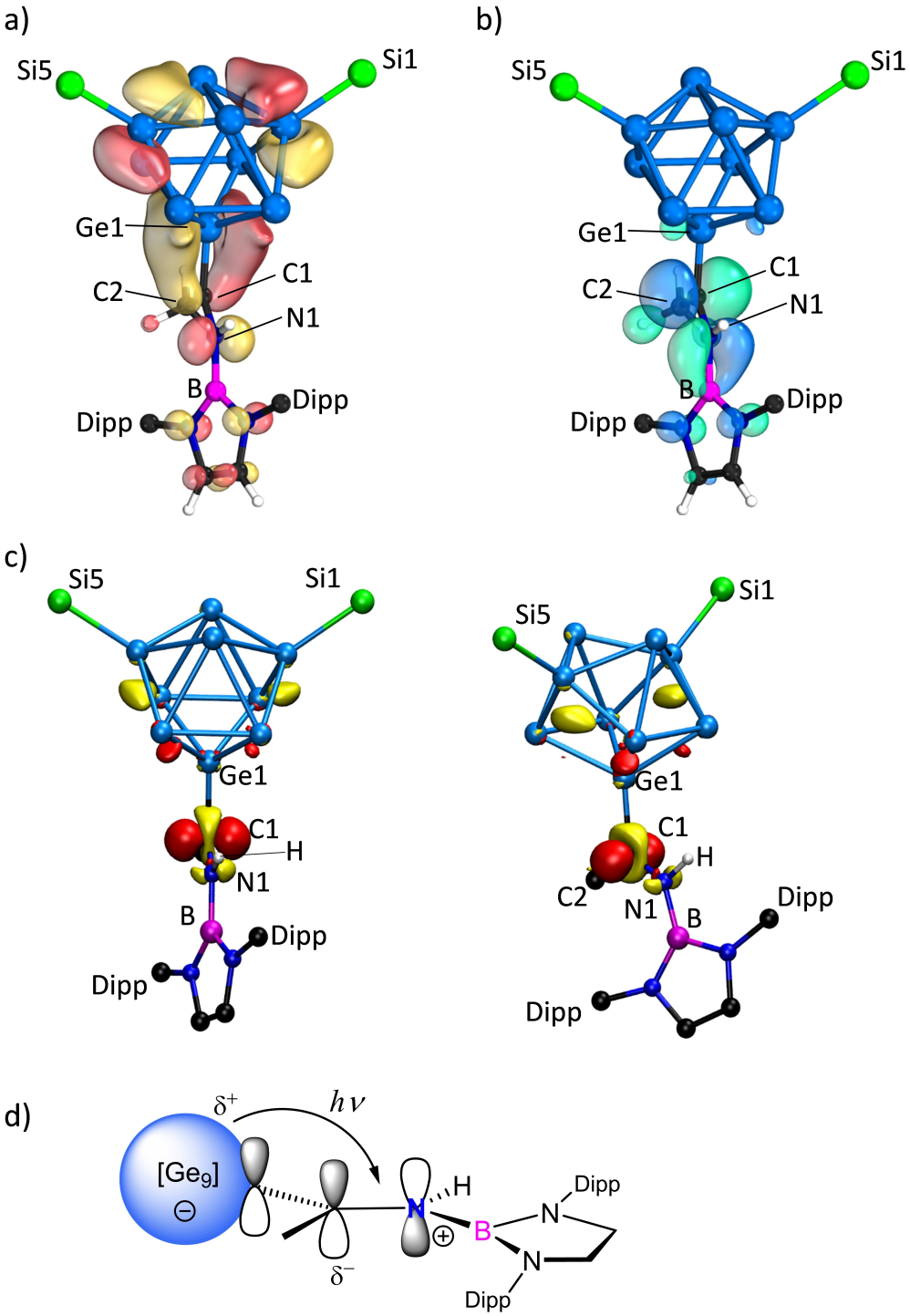

Figure 5. a) and b) Molecular orbitals of **1-H** calculated at the DFT-BP86/TZVP level of theory. a) Representation of the HOMO distributed over [Ge_9] and C1; b) representation of the LUMO dominated by the anti-bonding π* orbital of the C=N double bond. Molecular orbital plots are drawn in such way that 50% of the density is enclosed within the isosurface, corresponding approximately to an isovalue of 0.04 a.u. Additional illustrations with ligands drawn in full are provided in Supporting Information Figure S34. c) Two orientations of the electron density difference plot (rotated by approximately 45°) for the $S_0 \rightarrow S_2$ excitation in **1-H** (calculated $\lambda = 669$ nm). Red and yellow color corresponds to increasing and decreasing electron density, respectively, during the electronic transition. The isovalue of the electron density isosurfaces is 0.002 a.u. d) Schematic illustration of the cluster-ligand charge transfer during the excitation. The [Ge_9] cluster in **1-H** is represented as a large, blue sphere.

Author Contributions

CW performed the experimental work and authored the manuscript. YS and AJK performed the quantum chemical calculations. FSG supported the crystallization of compounds **1-K** and **1-H**. AK performed the TA measurements. ET and AK analysed TA data. JH and TFF supervised the project.

Acknowledgements

The authors thank the Deutsche Forschungsgemeinschaft (DFG, German Research Foundation, project number 245845833) within the International Research Training Group IRTG 2022 (ATUMS) for financial support and the Bavarian State Ministry of Science and the Arts for funding this work in the scope of the project "Solar Technologies go Hybrid". E.T. and J.H. acknowledge funding by the DFG-TRR 325-444632635. A.K. and J.H. acknowledge funding from the DFG through the excellence cluster *e*-conversion, under Germany's Excellence Strategy—EXC 2089/1—390776260. CW thanks the Studienstiftung des Deutschen Volkes for granting a PhD scholarship. A.J.K. thanks the Academy of Finland for funding (grant 340584) and CSC, the Finnish IT Center for Science for computational resources. The authors thank Dr. Max Schütz and M. Sc. Maximilian Muhr (Chair of Inorganic and Metal-Organic Chemistry, Prof. Fischer, TUM) for the acquisition of the LIFDI-MS data. Furthermore, the authors thank M. Sc. Lukas Niederegger (Chair of Bioinorganic Chemistry, Prof. Hess, TUM) for his help concerning all technical aspects of the UV/Vis measurements. M. Sc. Philipp Keil (Dr. Terrance Hadlington, TUM) is acknowledged for the acquisition of variable temperature NMR data and Dr. W. Klein supported the crystallographic part. Open Access funding enabled and organized by Projekt DEAL.

Conflict of Interest

The authors declare no conflict of interest.

Data Availability Statement

The data that support the findings of this study are available in the Supporting Information of this article.

Keywords: Charge Transfer · Chromophore · Germanium Cluster · Laser Irradiation · Synthesis

[1] O. Ito, F. D'Souza, *Molecules* **2012**, *17*, 5816.
[2] N. Zarrabi, C. Agatemor, G. N. Lim, A. J. Matula, B. J. Bayard, V. S. Batista, F. D'Souza, P. K. Poddutoori, *J. Phys. Chem. C* **2018**, *122*, 131.
[3] T. F. Fässler, *Angew. Chem. Int. Ed.* **2001**, *40*, 4161.
[4] "Discrete and Linked Homoatomic Clusters of the Elements Ge, Sn, and Pb": T. F. Fässler in *Metal Clusters in Chemistry*, Wiley-VCH, Weinheim, **2000**, ISBN: 9783527295494.
[5] M. M. Bentlohner, W. Klein, Z. H. Fard, L. A. Jantke, T. F. Fässler, *Angew. Chem. Int. Ed.* **2015**, *54*, 3748.
[6] M. M. Bentlohner, S. Frischhut, T. F. Fässler, *Chem. Eur. J.* **2017**, *23*, 17089.
[7] S. Frischhut, M. M. Bentlohner, W. Klein, T. F. Fässler, *Inorg. Chem.* **2017**, *56*, 10691.
[8] C. Wallach, F. S. Geitner, A. J. Karttunen, T. F. Fässler, *Angew. Chem. Int. Ed.* **2021**, *60*, 2648.
[9] O. Kysliak, T. Kunz, A. Schnepf, *Eur. J. Inorg. Chem.* **2017**, 805.
[10] K. Mayer, L. J. Schiegerl, T. Kratky, S. Günther, T. F. Fässler, *Chem. Commun.* **2017**, *53*, 11798.
[11] O. Kysliak, A. Schnepf, *Z. Anorg. Allg. Chem.* **2019**, *645*, 335.
[12] F. S. Geitner, J. V. Dums, T. F. Fässler, *J. Am. Chem. Soc.* **2017**, *139*, 11933.
[13] F. S. Geitner, C. Wallach, T. F. Fässler, *Chem. Eur. J.* **2018**, *24*, 4103.
[14] C. Wallach, F. S. Geitner, W. Klein, T. F. Fässler, *Chem. Eur. J.* **2019**, *25*, 12349.
[15] O. Kysliak, C. Schrenk, A. Schnepf, *Inorg. Chem.* **2017**, *56*, 9693.
[16] F. S. Geitner, W. Klein, T. F. Fässler, *Angew. Chem. Int. Ed.* **2018**, *57*, 14509.
[17] C. B. Benda, H. He, W. Klein, M. Somer, T. F. Fässler, *Z. Anorg. Allg. Chem.* **2015**, *641*, 1080.
[18] L. Yong, S. D. Hoffmann, T. F. Fässler, *Z. Anorg. Allg. Chem.* **2004**, *630*, 1977.
[19] L. Xu, S. C. Sevov, *J. Am. Chem. Soc.* **1999**, *121*, 9245.
[20] K. Mayer, W. Klein, S. Geier, T. F. Fässler, *Z. Anorg. Allg. Chem.* **2021**, *647*, 377.
[21] C. Downie, Z. Tang, A. M. Guloy, *Angew. Chem. Int. Ed.* **2000**, *39*, 337.
[22] C. Downie, J.-G. Mao, H. Parmar, A. M. Guloy, *Inorg. Chem.* **2004**, *43*, 1992.
[23] S. Frischhut, J. G. Machado de Carvalho, A. J. Karttunen, T. F. Fässler, *Z. Anorg. Allg. Chem.* **2018**, *644*, 1337.
[24] M. Klinger, C. Schenk, F. Henke, A. Clayborne, A. Schnepf, A.-N. Unterreiner, *Chem. Commun.* **2015**, *51*, 12278.
[25] N. C. Michenfelder, C. Gienger, M. Dilanas, A. Schnepf, A.-N. Unterreiner, *Molecules* **2020**, *25*, 2639.
[26] N. C. Michenfelder, C. Gienger, A. Schnepf, A.-N. Unterreiner, *Dalton Trans.* **2019**, *48*, 15577.
[27] C. Wallach, F. S. Geitner, T. F. Fässler, *Chem. Sci.* **2021**, *12*, 6969.
[28] M. Muhr, P. Heiß, M. Schütz, R. Bühler, C. Gemel, M. H. Linden, H. B. Linden, R. A. Fischer, *Dalton Trans.* **2021**, *50*, 9031.
[29] Deposition Numbers 2161506 (for **1-K**) and 2161507 (for **1-H**) contain the supplementary crystallographic data for this paper. These data are provided free of charge by the joint Cambridge Crystallographic Data Centre and Fachinformationszentrum Karlsruhe Access Structures service.
[30] O. Kysliak, A. Schnepf, *Dalton Trans.* **2016**, *45*, 2404.
[31] F. Li, S. C. Sevov, *Inorg. Chem.* **2012**, *51*, 2706.
[32] F. H. Allen, O. Kennard, D. G. Watson, L. Brammer, A. G. Orpen, R. Taylor, *J. Chem. Soc. Perkin Trans. 2* **1987**, S1.
[33] J. Barrau, J. Escudie, J. Satge, *Chem. Rev.* **1990**, *90*, 283.
[34] F. Meiners, W. Saak, M. Weidenbruch, *Organometallics* **2000**, *19*, 2835.
[35] T. L. Windus, M. S. Gordon, *J. Am. Chem. Soc.* **1992**, *114*, 9559.
[36] M. W. Hull, A. Ugrinov, I. Petrov, S. C. Sevov, *Inorg. Chem.* **2007**, *46*, 2704.

[37] L. Szi-Ferenc, Z. Csaszar, G. R. Lendvay, A. Benyei, S. Balogh, B. Nanasi, G. Farkas, J. Bakos, *Organometallics* **2018**, *37*, 2203.
[38] E. V. Anslyn, D. A. Dougherty, E. V. Dougherty, *Modern Physical Organic Chemistry*, University Science Books, Sausalito, **2006**, ISBN 9781891389313.
[39] F. S. Kocak, D. O. Downing, P. Zavalij, Y.-F. Lam, A. N. Vedernikov, B. Eichhorn, *J. Am. Chem. Soc.* **2012**, *134*, 9733.
[40] A. D. Becke, *Phys. Rev. A* **1988**, *38*, 3098.
[41] F. Furche, R. Ahlrichs, *J. Phys. Chem.* **2002**, *117*, 7433.
[42] "Density Functional Methods for Excited States: Equilibrium Structure and Electronic Spectra": F. Furche, D. Rappoport in *Computational Photochemistry, Vol. 16*, Elsevier, Amsterdam, **2005**, ISBN: 9780080455198.
[43] F. Weigend, R. Ahlrichs, *Phys. Chem. Chem. Phys.* **2005**, *7*, 3297.
[44] J. P. Perdew, *Phys. Rev. B* **1986**, *33*, 8822.
[45] I. H. van Stokkum, D. S. Larsen, R. Van Grondelle, *Biochim. Biophys. Acta Bioenerg.* **2004**, *1657*, 82.
[46] A. Dreuw, M. Head-Gordon, *Chem. Rev.* **2005**, *105*, 4009.

Manuscript received: March 24, 2023
Accepted manuscript online: April 27, 2023
Version of record online: June 13, 2023